available at www.sciencedirect.com
journal homepage: www.eu-openscience.europeanurology.com

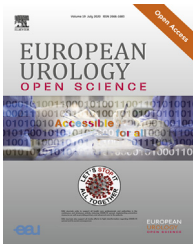

European Association of Urology

Urothelial Cancer

Prediction of Metastatic Patterns in Bladder Cancer: Spatiotemporal Progression and Development of a Novel, Web-based Platform for Clinical Utility

Jeremy Mason [a,b,e,*], *Zaki Hasnain* [c], *Gus Miranda* [a], *Karanvir Gill* [d], *Hooman Djaladat* [a], *Mihir Desai* [a], *Paul K. Newton* [c,e,f], *Inderbir S. Gill* [a,e], *Peter Kuhn* [a,b,c,d,e,f,g]

[a] *USC Institute of Urology, Catherine & Joseph Aresty Department of Urology, Keck School of Medicine, University of Southern California, Los Angeles, CA, USA;* [b] *Convergent Science Institute in Cancer, Michelson Center for Convergent Bioscience, University of Southern California, Los Angeles, CA, USA;* [c] *Department of Aerospace and Mechanical Engineering, Viterbi School of Engineering, University of Southern California, Los Angeles, CA, USA;* [d] *Department of Biological Sciences, Dornsife College of Letters, Arts, and Sciences, University of Southern California, Los Angeles, CA, USA;* [e] *Norris Comprehensive Cancer Center, Keck School of Medicine, University of Southern California, Los Angeles, CA, USA;* [f] *Department of Mathematics, University of Southern California, Los Angeles, CA, USA;* [g] *Department of Biomedical Engineering, Viterbi School of Engineering, University of Southern California, Los Angeles, CA, USA*

Article info

Article history:
Accepted July 19, 2021

Associate Editor:
Guillaume Ploussard

Keywords:
Metastasis
Metastatic patterns
Bladder cancer
Prediction
Spatiotemporal progression

Abstract

Background: Bladder cancer (BCa), the sixth commonest cancer in the USA, is highly lethal when metastatic. Spatial and temporal patterns of patient-specific metastatic spread are deemed random and unpredictable. Whether BCa metastatic patterns can be quantified and predicted more accurately is unknown.
Objective: To develop a web-based calculator for forecasting metastatic progression in individual BCa patients.
Design, setting, and participants: We used a prospectively collected longitudinal dataset of 3503 BCa patients who underwent a radical cystectomy following diagnosis and were enrolled continuously. We subdivided patients by their pathologic subgroup stages of organ confined (OC), extravesical (EV), and node positive (N+). We illustrated metastatic pathway progression using color-coded, circular, tree ring diagrams. We created a dynamical, data-visualization, web-based platform that displays temporal, spatial, and Markov modeling figures with predictive capability.
Outcome measurements and statistical analysis: Patients underwent history and physical examination, serum studies, and liver function tests. Surveillance follow-up included computed tomography scans, chest x-rays, and radiographic evaluation of the reservoir and upper tracts, with bone scans performed only if clinically indicated. Outcomes were measured by time to clinical recurrence and overall or progression-free survival.

* Corresponding author. University of Southern California, 1002 Childs Way, MCB 353, Los Angeles, CA 90089, USA. Tel.: +1-323-764-7965.
E-mail address: masonj@usc.edu (J. Mason).

http://dx.doi.org/10.1016/j.euros.2021.07.006

Results and limitations: Metastases developed in 29% of patients (n = 812; median follow-up 15.3 yr), with 5-yr overall survival of 20.2%, compared with 78.6% in those without metastases (n = 1983; median follow-up 10.9 yr). The three commonest sites of spread at the time of first progression were bone (n = 214; 26.4%), pelvis (n = 194; 23.9%), and lung (n = 194; 23.9%). The order and frequency of these sites vary when divided by pathologic subgroup stages of OC (lung [n = 65; 25.1%], urethra [n = 45; 17.4%], and bone [n = 29; 11.2%]), EV (pelvis [n = 63; 33.0%], bone [n = 45; 23.6%], and lung [n = 29; 15.2%]), and N+ (bone [n = 111; 30.7%], retroperitoneum [n = 70; 19.3%], and pelvis [n = 60; 16.6%]). Markov chain modeling indicated a higher probability of spread from bladder to bone (15.5%), pelvis (14.7%), and lung (14.2%).

Conclusions: Our web-based calculator allows real-time analyses in the clinic based on individual patient-specific demographic and cancer data elements. For contrasting subgroups, the models indicated differences in Markov transition probabilities. Spatiotemporal patterns of BCa metastasis and sites of spread indicated underlying organotropic mechanisms in the prediction of response. This recognition opens the possibility of organ site–specific therapeutic targeting in the oligometastatic BCa setting. In the precision medicine era, visualization of complex, time-resolved clinical data will enhance management of postoperative metastatic BCa patients.

Patient summary: We developed a web-based calculator to forecast metastatic progression for individual bladder cancer (BCa) patients, based on the clinical and demographic information obtained at diagnosis. This can help in predicting disease status and survival, and improving management in postoperative metastatic BCa patients.

1. Introduction

With an estimated 81 400 new cases in 2020, bladder cancer (BCa) is the sixth commonest cancer in the USA, accounting for approximately 4.7% of all estimated new cancer diagnoses (1 806 590) [1]. Despite advances in early diagnosis [2–7] and improved surgical and medical therapies [8–11], BCa is highly lethal in the metastatic setting, causing an estimated 17 980 deaths in 2020, of which only a minority are initially diagnosed with stage IV disease [1]. Throughout the course of the disease, various, still poorly understood, factors (environmental, biological, and host) drive progression and long-term survival [12–17].

Patterns and anatomic locations of metastatic spread from BCa are generally deemed random and unpredictable. Although certain sites (eg, lung) are more common than others (eg, brain), chronologic timing and lethality implications of site-specific metastases remain largely unknown [18,19]. Recent work by Shou et al [20] investigate the prognostic effect of specific combinations of metastases (bone, lung, liver, and brain) on overall survival. It was found that bone metastasis was the commonest single-site metastasis, while liver metastases provided the worst survival outcomes [20]. Still, many clinically relevant and important questions are currently unanswerable, such as the incidence of first metastasis to various sites (liver, lungs, and bones) and whether there is a site-specific timing differential. Equally, it is unknown whether different metastatic sites portend different cancer-specific survival and whether the histologic and cellular characteristics of the primary lesion impact the location of first metastasis. It is also unclear whether, in patients with oligometastatic disease, chemotherapy has differential efficacy based on the location of the metastatic site.

More predictable, granular, and systemic knowledge of BCa metastatic patterns, especially when correlated with histologic data, would be a first step toward developing patient-specific predictive models. Especially when combined with molecular and genetic data, this can guide the development of targeted therapies for disease-specific subgroups. While statistical forecasting tools are used routinely in certain fields (meteorology [21] and finance [22]), their application to precision medicine is still nascent. A few groups, including ours, have established initial mathematical models of metastasis performed on single time-point data across the main carcinomas. More recently, advanced models with time-resolved data in breast and lung cancer have been built [23–26], but have yet to be applied to BCa.

Herein, we developed a spatiotemporal forecasting calculator from a prospectively collected legacy database of 3503 primary BCa patients over a 45-yr period (1971–2016). To our knowledge, these are the first predictive models that attempt to forecast metastatic progression in individual BCa patients.

Table 1 – Patient and tumor characteristics for all patients stratified by pathologic stage subgroup

	All (*n* = 2795)	Organ confined (*n* = 1617)	Extravesical (*n* = 545)	Node positive (*n* = 633)
Decade of cystectomy, *n* (%)				
1970–1980	117 (4.2)	74 (4.6)	10 (1.8)	33 (5.2)
1980–1990	495 (17.7)	296 (18.3)	105 (19.3)	94 (14.8)
1990–2000	567 (20.3)	299 (18.5)	126 (23.1)	142 (22.4)
2000–2010	884 (31.6)	505 (31.2)	182 (33.4)	197 (31.1)
2010–2020	732 (26.2)	443 (27.4)	122 (22.4)	167 (26.4)
Age (yr)				
Median	68	67	70	68
Min-max	23–95	27–95	23–93	37–94
Gender, *n* (%)				
Female	574 (20.5)	302 (18.7)	118 (21.7)	154 (24.3)
Male	2221 (79.5)	1315 (81.3)	427 (78.3)	479 (75.7)
Radiation, *n* (%)				
Neoadjuvant	152 (5.4)	98 (6.1)	20 (3.7)	34 (5.4)
Adjuvant	20 (0.7)	4 (0.2)	7 (1.3)	9 (1.4)
Chemotherapy, *n* (%)				
Neoadjuvant	334 (11.9)	183 (11.3)	62 (11.4)	89 (14.1)
Adjuvant	506 (18.1)	59 (3.6)	131 (24.0)	316 (49.9)
Smoker, *n* (%)				
Current	543 (19.4)	289 (17.9)	110 (20.2)	144 (22.7)
Never	626 (22.4)	359 (22.2)	118 (21.7)	149 (23.5)
Previous	1528 (54.7)	908 (56.2)	306 (56.1)	314 (49.6)
Grade, *n* (%)				
0	69 (2.5)	64 (4)	4 (0.7)	1 (0.2)
1	2424 (86.7)	1272 (78.7)	540 (99.1)	612 (96.7)
2	302 (10.8)	281 (17.4)	1 (0.2)	20 (3.2)
Lymphovascular invasion, *n* (%)				
Positive	2004 (71.7)	1447 (89.5)	352 (64.6)	205 (32.4)
Negative	791 (28.3)	170 (10.5)	193 (35.4)	428 (67.6)
Survival status, *n* (%)				
Deceased	1620 (58.0)	794 (49.1)	349 (64.0)	477 (75.4)
Deceased by disease	701 (25.1)	203 (12.6)	171 (31.4)	327 (51.7)
Censored	1175 (42.0)	823 (50.9)	196 (36.0)	156 (24.6)
Progressed	812 (29.1)	259 (16.0)	191 (35.0)	362 (57.2)
Developed progression, *n* (%)				
Urethra	74 (2.6)	49 (3.0)	17 (3.1)	8 (1.3)
Pelvis	213 (7.6)	49 (3.0)	67 (12.3)	97 (15.3)
Lymph node (regional)	97 (3.5)	33 (2.0)	11 (2.0)	53 (8.4)
Lymph node (distal)	76 (2.7)	19 (1.2)	9 (1.7)	48 (7.6)
Peritoneum	59 (2.1)	13 (0.8)	9 (1.7)	37 (5.8)
Adrenal gland	30 (1.1)	5 (0.3)	9 (1.7)	16 (2.5)
Liver	198 (7.1)	53 (3.3)	47 (8.6)	98 (15.5)
Bone	259 (9.3)	67 (4.1)	67 (12.3)	125 (19.7)
Brain	47 (1.7)	15 (0.9)	13 (2.4)	19 (3.0)
Lung	228 (8.2)	81 (5.0)	59 (10.8)	88 (13.9)
Retroperitoneum	171 (6.1)	48 (3.0)	22 (4.0)	101 (16.0)
Upper tract	57 (2.0)	42 (2.6)	8 (1.5)	7 (1.1)
Other	133 (4.8)	42 (2.6)	27 (5.0)	64 (10.1)
Total developed progressions, *n* (%)				
0	1983 (70.9)	1358 (84.0)	354 (65.0)	271 (42.8)
1	370 (13.2)	126 (7.8)	88 (16.1)	156 (24.6)
2	223 (8.0)	63 (3.9)	56 (10.3)	104 (16.4)
3	121 (4.3)	35 (2.2)	32 (5.9)	54 (8.5)
4	52 (1.9)	20 (1.2)	8 (1.5)	24 (3.8)
5	28 (1.0)	12 (0.7)	5 (0.9)	11 (1.7)
6	11 (0.4)	2 (0.1)	2 (0.4)	7 (1.1)
7	7 (0.3)	1 (0.1)	0 (0)	6 (0.9)

The metastasis section represents the distinct number of patients who developed that particular progression, not counting multiple or repeat occurrences.

2. Patients and methods

2.1. Study design

We retrospectively analyzed an established, IRB-approved, longitudinally maintained, legacy radical cystectomy database of consecutive BCa primary surgical cases at our institution, the University of Southern California, containing prospectively collected, detailed clinical, radiologic, and pathologic elements dating back to August 1971. A total of 3503 consecutive patients were identified from the database who underwent radical cystectomy between August 1971 and February 2016 (median follow-up 11.5 yr; range 0–39 yr). In order to examine a homogeneous cohort, similar to that studied by Stein et al [8], we report on only those with urothelial carcinoma histology treated with intent to cure (*n* = 2795; median follow-up 11.6 yr; range 0–39 yr). Non-BCa primary patients undergoing cystectomy for other pelvic malignancies

were excluded. Patients receiving neoadjuvant chemotherapy (n = 334; 16.5%) were included. Patients were divided into pathologic subgroups of organ confined (OC; lymph node–negative tumors and <pT3), non-OC/extravesical (EV; lymph node–negative tumors and pT3–4), and node positive (N+; lymph node–positive tumors irrespective of T staging). Additional cohort statistics can be found in Table 1. Full details can be found in Supplementary Table 1. It is important to note that it is routine surgical practice at our institution to remove a significant number of lymph nodes in an extended fashion (average 40.2 per patient) during radical cystectomy.

Patients were typically followed at 3–6-mo intervals for the first 2 yr and annually thereafter. Routine studies included a thorough history and physical examination, serum studies, including the monitoring of electrolyte and creatinine levels, and liver function tests. Computed tomography (CT) scans, chest x-rays, and radiographic evaluation of the reservoir and upper tracts (by intravenous pyelography, and ultrasound and/or pouch/cystogram, as appropriate) were done as surveillance follow-ups. Bone scans were performed only if clinically indicated. While current imaging techniques for primary BCa (cT staging) are notoriously inaccurate with a ~50% understaging rate [27–30], this level of inaccuracy has remained largely unchanged throughout the years; this minimizes the imaging bias between the earlier and more recently treated patients. We rely on the expertise of the radiologists and other physicians to identify and classify metastatic lesions correctly.

Outcomes were measured by time to recurrence and overall survival. Time to clinical recurrence or progression-free survival was calculated as the time from cystectomy to the date of first documented clinical recurrence, or until the last follow-up if the patient had not experienced a clinical recurrence. Patients who died before clinical recurrence were censored at the time of death. Overall survival was calculated as the time from cystectomy to death. All deaths, regardless of cause, were counted as events; patients who are still alive were censored at the date of last contact. Additionally, as this study was started before the advent of genomic sequencing, no downstream analyses were performed. The availability of archived formalin-fixed paraffin-embedded blocks would provide a future opportunity to map genetic traits with progression patterns.

2.2. Web platform

The spatiotemporal forecasting calculator (http://kuhn.usc.edu/bladder_cancer/) was developed as a (near) real-time learning tool for patients, clinicians, and researchers, allowing for real-time prognostication on an individual patient basis by mapping metastatic disease. The user self-selects patient descriptors of interest based on the available dataset(s). After selection, a column of figures is generated that can be matched side by side with a contrasting group(s), allowing for user analysis and discoveries. More details of the web platform can be found in the Supplementary material.

2.3. Metastatic probability

The probability of BCa progression is calculated as a time-dependent exponential decay function measured from the date of cystectomy. Individual probabilities are calculated at each time point as the number of metastatic patients who have not yet progressed, divided by the total number of patients still at risk of progression. At-risk patients are those who do not have metastatic disease at that time and are still in the study (not deceased and not left study). The calculated data points are then fitted to an exponential decay function.

2.4. Spatiotemporal data display

BCa progression was analyzed via spatiotemporal tree ring diagrams that depict step-by-step transitions between sites. Color-coded sites allow for quick and easy detection of progression patterns within the cohort and subsets based on clinical and demographic stratification. Temporal evolution of progression was analyzed by generating tree rings that are "frozen" at specific time points after cystectomy. More details on these diagrams can be found in the Supplementary material.

2.5. Markov modeling

BCa progression was simulated via Monte Carlo simulations of random walkers on Markov chain networks constructed from progression pathways. Similar to the spatiotemporal display, subsets of patients can be used to create targeted networks to predict for specific populations. More details on these models can be found in the Supplementary material.

3. Results

Our analysis included 2795 patients with urothelial BCa in our dataset. Of these patients, 2221 (79.5%) were men and 574 (20.5%) were women. The median age at diagnosis was 68 yr (range: 23–95 yr).

3.1. Overall survival and metastatic potential

We analyzed temporal patterns of 2795 primary urothelial BCa patients. Of these patients, 812 (29.1%) developed clinically detectable distant metastases and were additionally analyzed for their spatial progression patterns. While there is a potential for the remaining 1983 patients to have developed subclinical metastases before death (n = 895) or leaving the study (n = 1088), we only report on those detected throughout the course of the patient's care. Figure 1A shows Kaplan-Meier survival curves for the metastatic and nonmetastatic populations after cystectomy. Radical cystectomy is used as time zero from which to calculate progression patterns. Figure 1B shows Kaplan-Meier survival curves for the metastatic and nonmetastatic populations stratified by pathologic subgroup stage. The metastatic EV and N+ cohorts fare far worse, with 5-yr overall survival rates of 15.1% and 7.2%, respectively. Overall survival rates after 10 yr remain relatively high for the nonmetastatic groups (OC: 66.8%; EV: 48.3%; N+: 53.1%) as compared with the metastatic groups (OC: 18.3%; EV: 6.0%; N+: 4.1%). Paired log-rank tests are shown in Table 2. Supplementary Figures 1A and 1B show the overall and progression-free survival, respectively, of these pathologic subgroup stages without stratifying by metastatic status. Paired log-rank tests for these curves are shown in Supplementary Tables 2 and 3.

We investigated the homogeneity of outcomes of the patients when divided by decade in which their cystectomy was performed. Supplementary Figure 1C, with paired Supplementary Table 4, shows the overall survival of these subgroups. These groups have an average 5-yr overall survival rate of 59.1% (standard deviation of 2.0%) and an average 10-yr overall survival rate of 45.0% (standard deviation of 1.3%). Supplementary Figure 1D, with paired Supplementary Table 5, shows the progression-free survival of these subgroups. These groups have an average 5-yr

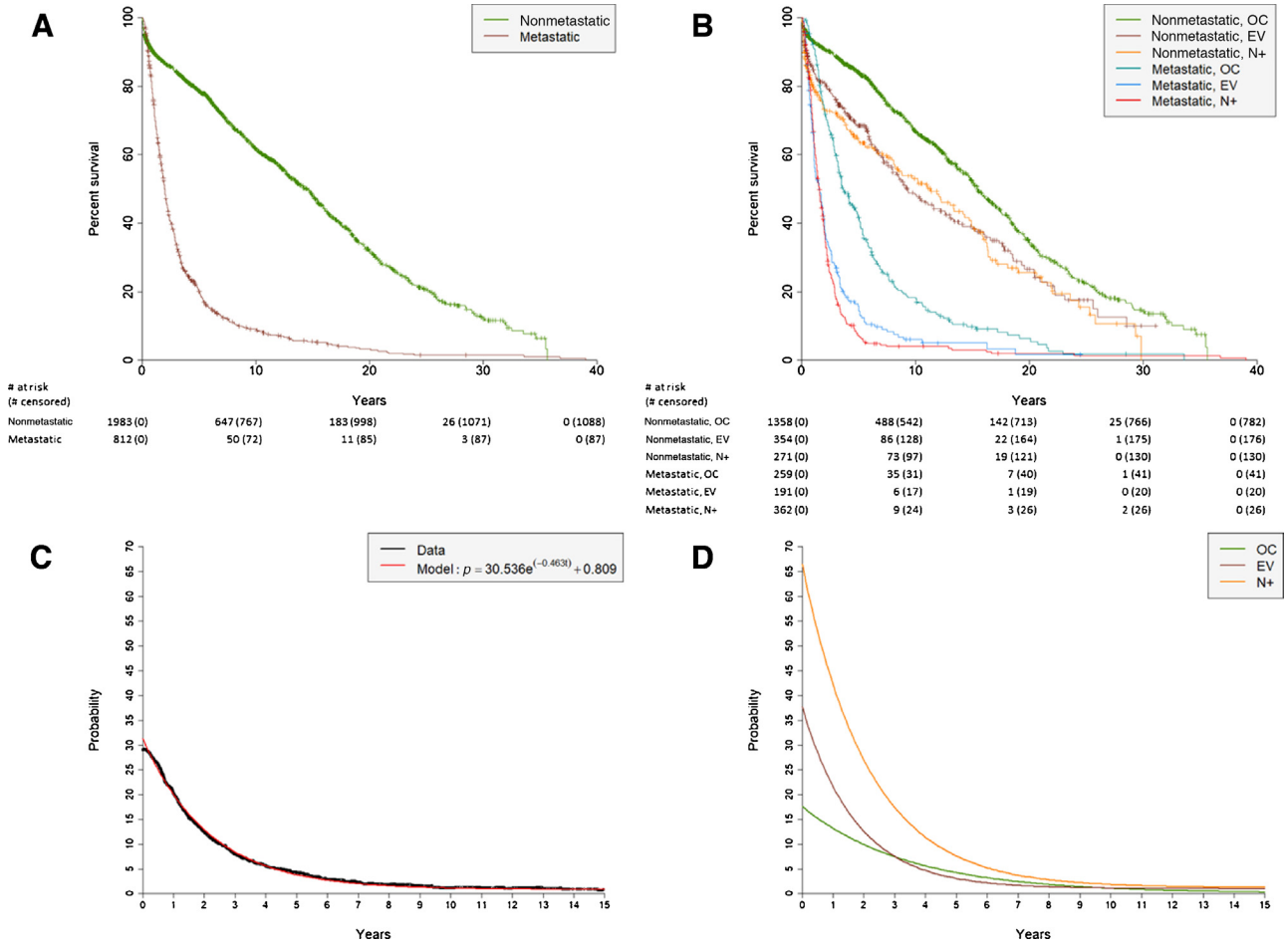

Fig. 1 – Kaplan-Meier curves of overall survival from the date of cystectomy over a 40-yr period for (A) metastatic and nonmetastatic patients and (B) metastatic and nonmetastatic patients stratified by pathologic subgroup stages of organ confined (OC), extravesical (EV), and node positive (N+). Probability curves of developing metastatic disease after cystectomy of primary BCa over time for (C) all patients and (D) patients stratified by pathologic subgroup stage. For the probability of developing metastatic disease for all patients (Fig. 1C), data points (black) are calculated as the number of metastatic patients who have not progressed yet divided by the total number of patients who are still at risk of progression. The probabilities are subsequently fit to an exponential decay function (red). An identical approach is taken for groups stratified by pathologic subgroup stage (Fig. 1D). BCa = bladder cancer.

progression-free survival rate of 66.9% (standard deviation of 2.9%) and an average 10-yr progression-free survival rate of 63.4% (standard deviation of 3.3%). Note that the most recent group, 2010–2020, is not included in the 10-yr averages due to a shorter follow-up time.

Figure 1C shows the time-dependent probability of primary BCa patients developing distant metastatic disease following cystectomy. Figure 1D shows the risk of metastasis based on the pathologic subgroup stage of patients. As expected, the OC subgroup has a much lower chance of progression early after cystectomy (16.0%) as compared with the EV (35.0%) and N+ (57.2%) subgroups. At the 5-yr mark, these probabilities are 4.1%, 3.9%, and 5.8%, respectively.

3.2. *Metastatic spatiotemporal progression*

Metastatic progression was most easily viewed as a collection of circular tree ring diagrams (Fig. 2). These show patterns of progression at 3, 6, and 9 mo and 1, 2, 3, 5, 10, and 15 yr after cystectomy. Immediately after surgery, patients are depicted as a brown ring for primary BCa, surrounded by an ivory ring representing no metastatic involvement (tree ring diagram not shown). Most metastatic progression occurs within the first 5 yr, as evidenced by the largely unchanged spatiotemporal diagrams in Figures 2G–I. Bone is the commonest site for BCa metastatic progression and is also the commonest first metastatic site ($n = 214$; 26.4%). The next frequent sites of spread at the time of first progression are pelvis ($n = 194$; 23.9%) and lung ($n = 194$; 23.9%).

Patients with first metastatic sites involving the brain or the peritoneum most frequently progressed to death before additional metastatic sites (80.0% and 84.6%, respectively). These findings contrast with the outcome of other metastatic sites such as the retroperitoneum (17.9%) and the upper tract (23.3%). As shown by Figure 2D, approximately half of the metastatic patients develop metastatic disease within 1 yr after cystectomy. Overall, Figure 2 demonstrates that a small proportion of patients experience

Table 2 – Statistical significance (*p* value) of paired log rank tests for subgroups of metastatic and nonmetastatic BCa patients stratified by pathologic subgroup stage of organ confined (OC), extravesical (EV), and node positive (N+; paired with Fig. 1B)

	Nonmetastatic, EV	Nonmetastatic, N+	Metastatic, OC	Metastatic, EV	Metastatic, N+
Nonmetastatic, OC	7.50E-08	5.41E-08	0	0	0
Nonmetastatic, EV	–	0.539	4.61E-14	0	0
Nonmetastatic, N+	–	–	9.06E-10	0	0
Metastatic, OC	–	–	–	7.35E-14	0
Metastatic, EV	–	–	–	–	0.140

BCa = bladder cancer.

single-site metastases followed by rapid progression to death; however, the majority of patients who die from BCa following cystectomy harbor multiple metastatic sites within a short time frame. It is important to note that while some sites represent local progression and others distant metastases, the combinations of sites can encompass distinct biological realities. The spatiotemporal model reported here utilizes a generalized approach in which all sites are treated in an unbiased manner without making any assumptions.

3.3. *Subset comparisons*

Exploring more deeply into these progression patterns, we divided the metastatic population based on its pathologic subgroups (OC, EV, and N+) and constructed their respective spatiotemporal diagrams for further analysis (Fig. 3). As seen, the distribution and patterns of metastatic sites differ vastly among the three groups, most notably in the first progression step. For OC patients, the most frequent sites of first progression are the lung (n = 65; 25.1%), urethra (n = 45; 17.4%), and bone (n = 29; 11.2%), while for EV patients, these are the pelvis (n = 63; 33.0%), bone (n = 45; 23.6%), and lung (n = 29; 15.2%) and for N+ patients, these are bone (n = 111; 30.7%), retro (n = 70; 19.3%), and pelvis (n = 60; 16.6%). When looking at all first sites, a total of 120 OC patients (46.3%) progress to death before developing additional metastases, compared with 85 EV patients (44.5%) and 152 N+ patients (42.0%). The average numbers of metastatic sites developed per patient are 2.2 for OC and N+ and 2.0 for EV.

3.4. *Markov chain network models*

Figure 4 depicts the graphical representation of the Markov chain network models that were constructed from the final pathway distributions of the subgroups shown in Figure 3. For all the models, the three commonest sites of first progression also have the highest transition probabilities from the bladder. The clockwise ordering, which is related to decreasing transition probabilities from primary BCa, is unique to each subgroup. In these figures, we omitted the "deceased" category to highlight the systemic nature of the disease, thus eliminating the notion of lethality for a site. This is done to acknowledge that the last metastatic site before death is not necessarily the cause of death.

4. Discussion

Our work demonstrates that the pattern of BCa metastatic spread from site to site is neither random nor unpredictable. This is even more striking when comparing distinct patient subgroups, as we have shown within the subsets stratified by pathologic subgroup. Furthermore, the characteristic patterns that define particular subgroups suggest that there may be underlying organotropic mechanisms at play that shape the metastatic landscape. As such, this encourages exploration of organ site–specific targeting therapies in the setting of oligometastatic disease, maximizing patient benefit.

Our metastatic spatiotemporal depictions identified the commonest and uncommonest sites of first metastasis and progression to other site(s), multiple metastasis and progression to other site(s), and their overall survival. Consistent with the recent publication by Shou et al [20], three of the commonest sites of spread were the bone, lung, and liver, with one of the uncommonest being the brain. This is also consistent with the findings of the previous studies conducted over the past 45 yr [31–36]. Additionally, progression patterns (site-to-site transitions) are identified easily via these diagrams. Side-by-side comparisons of contrasting subgroups allow for quick identification and understanding of biological/clinical drivers within each group and their effect on overall survival.

4.1. *Clinical implications/results in context*

Incorporating the Markov model, we can identify which patients develop the next site of solitary or multiple metastases with decreasing strength of transition probability. Stratifying by demographic, clinical, and pathologic stage/subgroups and use of chemotherapy parameters, targeted model building allows site-specific prediction for targeted subgroups. For the first time, we begin to see which type of BCa primary has predilection for metastasizing to one site versus another. Thus, the most probable sites of spread are also, in reality, the commonest sites of spread (bone, pelvis, and lung), which intuitively makes sense. Additionally, we can utilize the model to map the most probable patterns of progression, starting with the commonest sites. For example, spread to the lung followed by the brain in OC patients has a 4.9% probability (15.6% ×

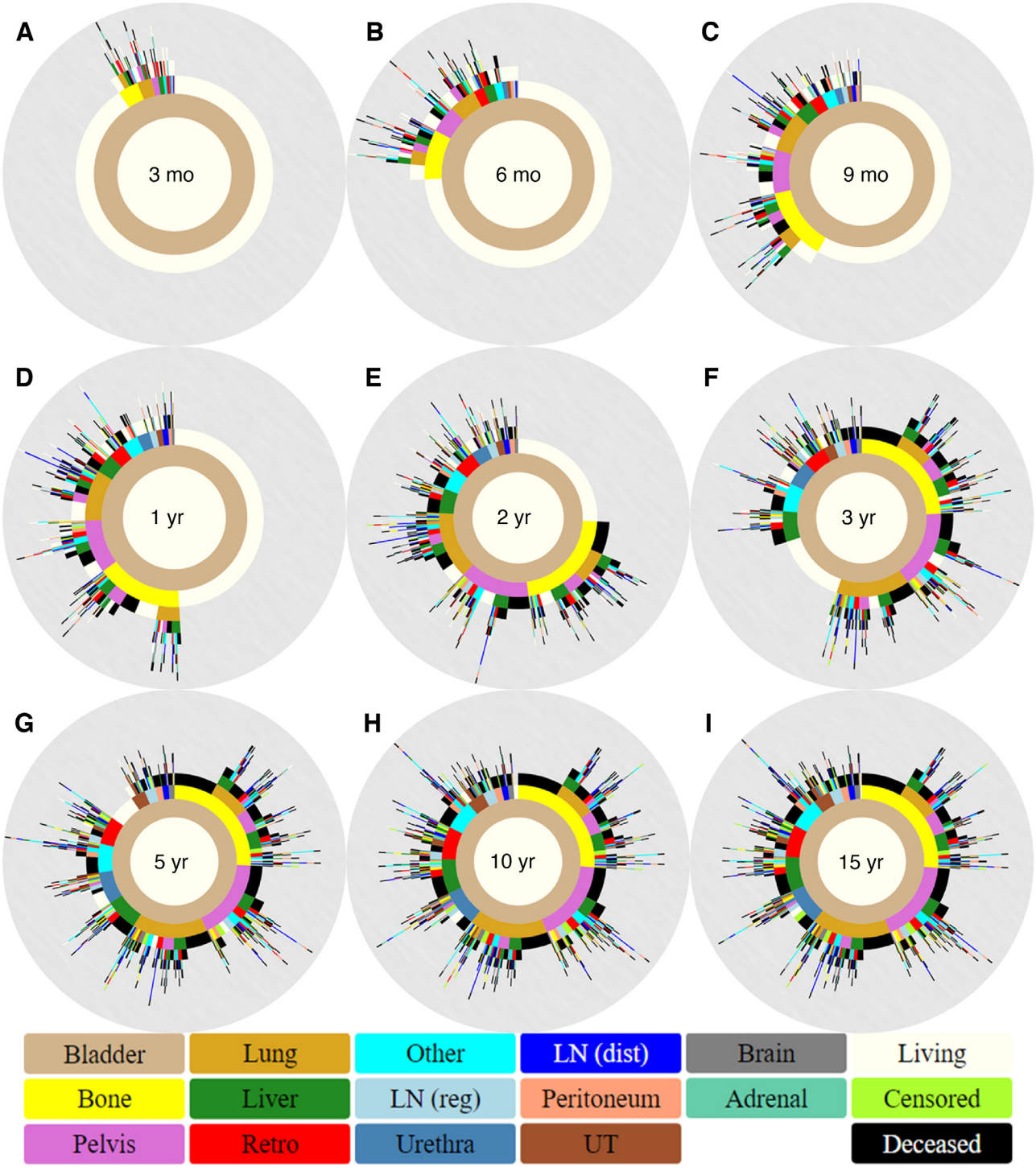

Fig. 2 – Spatiotemporal progression diagrams for (A) 3 mo, (B) 6 mo, (C) 9 mo, (D) 1 yr, (E) 2 yr, (F) 3 yr, (G) 5 yr, (H) 10 yr, and (I) 15 yr after cystectomy. Sites of spread include the bone, pelvis, lung, liver, Retro, "LN (reg)", urethra, "LN (dist)", peritoneum, UT, brain, and adrenal gland. Pelvis refers to pelvic soft tissue, Retro to the retroperitoneum, LN (reg) to regional lymph nodes, LN (dist) to distant lymph nodes, and UT to the upper tract. Other is reserved for any infrequent metastasis that does not fall in the other major categories. Markers for a patient's overall survival status being living, deceased, or censored are also included.

31.6%), spread to the pelvis followed by the liver in EV patients has a 5.9% probability (21.1% × 27.8%), and spread to the bone followed by regional lymph node in N+ patients has a 5.9% probability (17.6% × 33.3%).

Our unique spatiotemporal forecasting calculator provides a novel opportunity to perform real-time analyses of focused primary BCa subgroups. The side-by-side design allows visualization of subtle differences between groups,

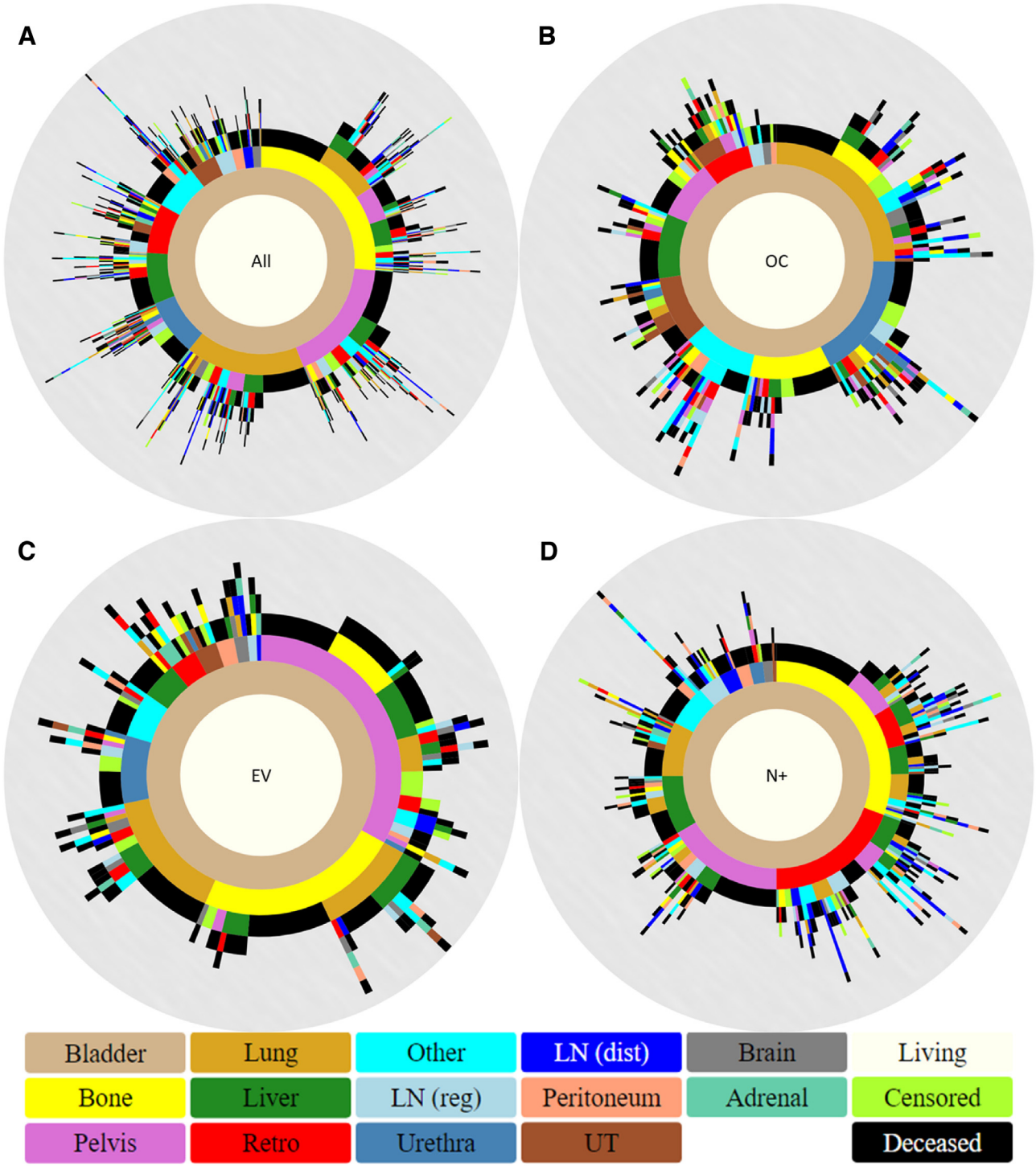

Fig. 3 – Spatiotemporal progression diagrams for (A) all metastatic patients, (B) OC metastatic patients, (C) EV metastatic patients, and (D) N+ metastatic patients. Pelvis refers to pelvic soft tissue, Retro to the retroperitoneum, LN (reg) to regional lymph nodes, LN (dist) to distant lymph nodes, and UT to the upper tract. Other is reserved for any infrequent metastasis that does not fall in the other major categories. EV = extravesical; N+ = node positive; OC = organ confined.

potentially tailoring therapies to individual patients. Additionally, the design allows patients, clinicians, or researchers to address disease relevant questions. We can now determine incidences of first metastases to key sites such as the liver, lungs, or bones, and whether there is differential timing of metastatic spread to these locations. Further, we can determine whether site-specific metastases portend different survival probabilities.

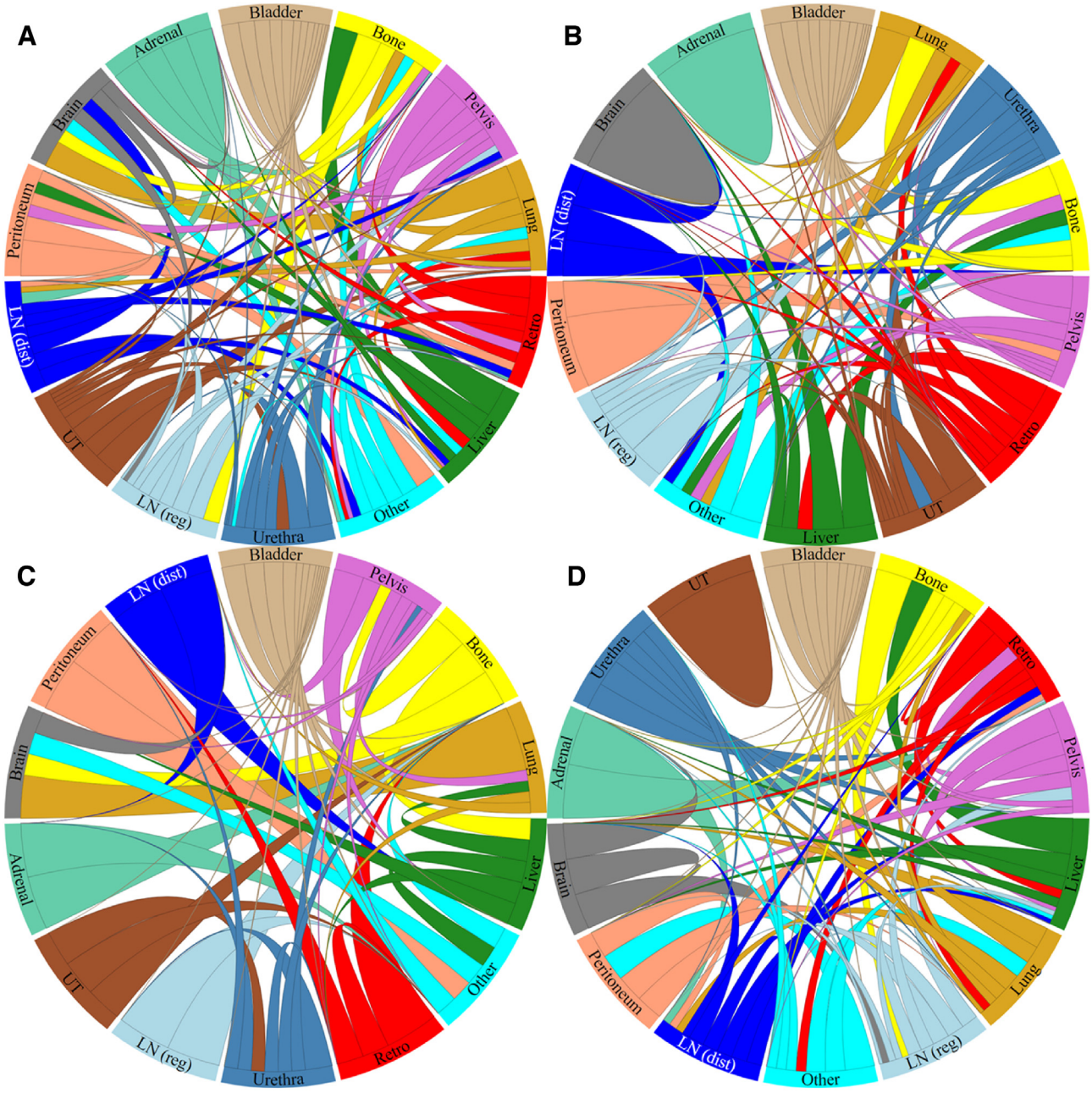

Fig. 4 – Markov chain diagrams for (A) all metastatic patients, (B) OC metastatic patients, (C) EV metastatic patients, and (D) N+ metastatic patients. EV = extravesical; N+ = node positive; OC = organ confined; LN (dist) = distant lymph nodes; LN (reg) = regional lymph nodes; Retro = retroperitoneum.

There are three main uses for our spatiotemporal calculator: (1) scientific discovery, (2) treatment development, and (3) therapy optimization. As we have shown, this tool can be used to track new findings within targeted subgroups of a population and between contrasting groups. The knowledge gained from such discoveries will highlight the intricacies of BCa and allow for more targeted approaches to treatment. With addition of longitudinal treatment information, pharmaceutical companies can track efficacy of specific drugs more easily. Lastly, our calculator can be used in the clinic in real time to optimize patient therapies based on demographic and cancer-specific data elements. This opens the door for clinicians to proactively understand the potential for response/failure from a proposed therapy. Leveraging the temporal data within the dataset will allow for more accurate timing of these events that typically cause most of the problems throughout the disease course.

4.2. Strengths and limitations/final considerations

Our prominent median follow-up time from a single institution in an intent-to-cure cohort gives confidence in predictive accuracy for long-term outcomes. Using this

homogenous group of patients with urothelial cancer, treated in a similar format over a long period of time, we can study the underlying biological mechanisms of spread, captured and modeled via commonplace models in use in other fields. Compared with our previous work, this current dataset has advantages of being larger with many more clinical variables (77+ vs 43, 22, and 49), with all patients having received the same standard of care (cystectomy), at a single institution, regardless of diagnosis and treatment dates, over a longer time range (45 vs 34, 36, and 8 yr). Importantly, the availability of the nonmetastatic counterpart allows new possibilities of developing machine learning algorithms [37].

Further improvement is possible. The accrual of 3503 patients in our current dataset is not a trivial endeavor, having prospectively been achieved continuously over a 45-yr period. Nonetheless, its relatively small total size is still a limiting factor. Upon stratification of each additional criterion, the subgroup further reduces its size and predictive power, thus decreasing forecasting accuracy. Addition of similar high-quality datasets from other leading centers will increase the number of patients, alleviating this problem. Another substantial step would be incorporating genomic data using archived tissue blocks, thus increasing prognostication accuracy at the individual patient level.

5. Conclusions

Ultimately, we anticipate that this tool will be used within the clinic and clinical research to help improve patient outcomes. Individualized forecasting based on patient-specific contextual data remains a challenge. While our models give a unique view of how populations of BCa progress based on certain demographic choices, they lack specific context at an individual patient level. Since real benefits would emerge at this higher resolution, development of patient-specific predictive models is necessary before clinical validation of our calculator can occur. Having a robust system that gracefully incorporates increasingly complex data, while maintaining the functionality and predictive power associated with the models, is important. As cancer research expands and more data become available over time, our calculator must be able to maintain its predictive power and improve, in order to avoid antiquation. Consequently, we plan to continually maintain our platform and externally validate with additional robust datasets.

Author contributions: Jeremy Mason had full access to all the data in the study and takes responsibility for the integrity of the data and the accuracy of the data analysis.

Study concept and design: Mason, Newton, I.S. Gill, Kuhn.
Acquisition of data: Miranda.
Analysis and interpretation of data: Mason, Hasnain.
Drafting of the manuscript: Mason, Miranda, K. Gill, Newton, I.S. Gill, Kuhn.
Critical revision of the manuscript for important intellectual content: Mason, Miranda, K. Gill, Djaladat, Desai, Newton, I.S. Gill, Kuhn.
Statistical analysis: Mason, Hasnain.
Obtaining funding: I.S. Gill, Kuhn.
Administrative, technical, or material support: None.
Supervision: Newton, I.S. Gill, Kuhn.
Other: None.

Financial disclosures: Jeremy Mason certifies that all conflicts of interest, including specific financial interests and relationships and affiliations relevant to the subject matter or materials discussed in the manuscript (eg, employment/affiliation, grants or funding, consultancies, honoraria, stock ownership or options, expert testimony, royalties, or patents filed, received, or pending), are the following: None.

Funding/Support and role of the sponsor: This work is funded in whole or in part by the NCI's USC Norris Comprehensive Cancer Center (CORE) Support (grant No. 5P30CA014089-40). This work also received institutional support from the USC Institute of Urology and the USC Convergent Science Institute in Cancer. This work was supported by grant KL2TR001854 from the National Center for Advancing Translational Science (NCATS) of the U.S. National Institutes of Health (JM). The content is solely the responsibility of the authors and does not necessarily represent the official views of the National Institutes of Health.

Acknowledgments: This prospective, longitudinal dataset is maintained by Gus Miranda and provided by the Catherine & Joseph Aresty Department of Urology and the USC Institute of Urology at the Keck School of Medicine at USC.

Appendix A. Supplementary data

Supplementary material related to this article can be found, in the online version, at doi:https://doi.org/10.1016/j.euros.2021.07.006.

References

[1] Siegel RL, Miller KD, Jemal A. Cancer statistics, 2020. CA Cancer J Clin 2020;70:7–30.
[2] Malmström PU. Why has the survival of patients with bladder cancer not improved? BJU Int 2008;101:267–9.
[3] Schmitz-Dräger BJ, Droller M, Lokeshwar VB, et al. Molecular markers for bladder cancer screening, early diagnosis, and surveillance: the WHO/ICUD consensus. Urol Int 2015;94:1–24.
[4] Shirodkar SP, Lokeshwar VB. Potential new markers in the early detection of bladder cancer. Curr Opin Urol 2009;19:488–93.
[5] Khadjavi A, Mannu F, Destefanis P, et al. Early diagnosis of bladder cancer through the detection of urinary tyrosine-phosphorylated proteins. Br J Cancer 2015;113:469–75.
[6] Fradet Y. Screening for bladder cancer: the best opportunity to reduce mortality. Can Urol Assoc J 2009;3(6 Suppl 4), S180–3.
[7] Grossman HB, Messing E, Soloway M, et al. Detection of bladder cancer using a point-of-care proteomic assay. JAMA 2005;293:810–6.
[8] Stein JP, Lieskovsky G, Cote R, et al. Radical cystectomy in the treatment of invasive bladder cancer: long-term results in 1,054 patients. J Clin Oncol 2001;19:666–75.

[9] Preston MA, Lerner SP, Kibel AS. New trends in the surgical management of invasive bladder cancer. Hematol Oncol Clin North Am 2015;29:253–69.
[10] Nguyen QT, Tsien RY. Fluorescence-guided surgery with live molecular navigation—a new cutting edge. Nat Rev Cancer 2013;13:653–62.
[11] Cheung G, Sahai A, Billia M, et al. Recent advances in the diagnosis and treatment of bladder cancer. BMC Med 2013;11:13.
[12] van Rhijn BW, Burger M, Lotan Y, et al. Recurrence and progression of disease in non–muscle-invasive bladder cancer: from epidemiology to treatment strategy. Eur Urol 2009;56:430–42.
[13] Millan-Rodriguez F, Chechile-Toniolo G, Salvador-Bayarri J, Palou J, Algaba F, Vicente-Rodríguez J. Primary superficial bladder cancer risk groups according to progression, mortality and recurrence. J Urol 2000;164:680–4.
[14] Fernandez-Gomez J, Solsona E, Unda M, et al. Prognostic factors in patients with non–muscle-invasive bladder cancer treated with bacillus Calmette-Guérin: multivariate analysis of data from four randomized CUETO trials. Eur Urol 2008;53:992–1001.
[15] Millan-Rodriguez F, Chechile-Toniolo G, Salvador-Bayarri J, Palou J, Vicente-Rodríguez J. Multivariate analysis of the prognostic factors of primary superficial bladder cancer. J Urol 2000;163:73–8.
[16] Bassi P, Ferrante Gd, Piazza N, et al. Prognostic factors of outcome after radical cystectomy for bladder cancer: a retrospective study of a homogeneous patient cohort. J Urol 1999;161:1494–7.
[17] Burger M, Catto JW, Dalbagni G, et al. Epidemiology and risk factors of urothelial bladder cancer. Eur Urol 2013;63:234–41.
[18] Hiensch R, Belete H, Rashidfarokhi M, Galperin I, Shakil F, Epelbaum O. Unusual patterns of thoracic metastasis of urinary bladder carcinoma. J Clin Imaging Sci 2017;7:23.
[19] Herr HW. Natural history of superficial bladder tumors: 10-to 20-year follow-up of treated patients. World J Urol 1997;15:84–8.
[20] Shou J, Zhang Q, Zhang D. The prognostic effect of metastasis patterns on overall survival in patients with distant metastatic bladder cancer: a SEER population-based analysis. World J Urol 2021. http://dx.doi.org/10.1007/s00345-021-03721-6.
[21] Pielke Sr RA. Mesoscale meteorological modeling, Vol. 98. Academic Press; 2013.
[22] Kumar D, Meghwani SS, Thakur M. Proximal support vector machine based hybrid prediction models for trend forecasting in financial markets. J Comput Sci 2016;17:1–13.
[23] In GK, Mason J, Lin S, et al. Development of metastatic brain disease involves progression through lung metastases in EGFR mutated non-small cell lung cancer. Converg Sci Phys Oncol 2017;3:034001.
[24] Newton PK, Mason J, Bethel K, et al. Spreaders and sponges define metastasis in lung cancer: a Markov chain Monte Carlo mathematical model. Cancer Res 2013;73:2760–9.
[25] Newton PK, Mason J, Bethel K, Bazhenova LA, Nieva J, Kuhn P. A stochastic Markov chain model to describe lung cancer growth and metastasis. PLoS One 2012;7:e34637.
[26] Newton PK, Mason J, Venkatappa N, et al. Spatiotemporal progression of metastatic breast cancer: a Markov chain model highlighting the role of early metastatic sites. NPJ Breast Cancer 2015;1:15018.
[27] MacVicar AD. Bladder cancer staging. BJU Int 2000;86(Suppl 1):111–22.
[28] Jewett HJ, Strong GH. Infiltrating carcinoma of the bladder: relation of depth of penetration of the bladder wall to incidence of local extension and metastases. J Urol 1946;55:366–72.
[29] McKibben MJ, Woods ME. Preoperative imaging for staging bladder cancer. Curr Urol Rep 2015;16:22.
[30] Lee CH, Tan CH, Faria SdC, et al. Role of imaging in the local staging of urothelial carcinoma of the bladder. Am J Roentgenol 2017;208:1193–205.
[31] Shinagare AB, Ramaiya NH, Jagannathan JP, Fennessy FM, Taplin ME, Van den Abbeele AD. Metastatic pattern of bladder cancer: correlation with the characteristics of the primary tumor. Am J Roentgenol 2011;196:117–22.
[32] Goldman SM, Fajardo AA, Naraval RC, Madewell JE. Metastatic transitional cell carcinoma from the bladder: radiographic manifestations. Am J Roentgenol 1979;132:419–25.
[33] Wallmeroth A, Wagner U, Moch H, et al. Patterns of metastasis in muscle-invasive bladder cancer (pT2–4): an autopsy study on 367 patients. Urol Int 1999;62:69–75.
[34] Kurian A, Lee J, Born A. Urothelial bladder cancer with cavitary lung metastases. Can Respir J 2011;18, e46–7.
[35] Salvati M, Cervoni L, Orlando ER, Delfini R. Solitary brain metastases from carcinoma of the bladder. J Neurooncol 1993;16:217–20.
[36] Whitmore WF, Batata MA, Ghoneim MA, Grabstald H, Unal A. Radical cystectomy with or without prior irradiation in the treatment of bladder cancer. J Urol 1977;118(1 Part 2):184–7.
[37] Hasnain Z, Mason J, Gill K, et al. Machine learning models for predicting post-cystectomy recurrence and survival in bladder cancer patients. PLoS One 2019;14:e0210976.